Resonant enhancement of second harmonic generation in the mid-infrared using localized surface phonon polaritons in sub-diffractional nanostructures

Ilya Razdolski,[*,†] Yiguo Chen,[‡,‖] Alexander J. Giles,[¶] Sandy Gewinner,[†] Wieland Schöllkopf,[†] Minghui Hong,[§] Martin Wolf,[†] Vincenzo Giannini,[‡] Joshua D. Caldwell,[¶] Stefan A. Maier,[‡] and Alexander Paarmann[*,†]

Fritz-Haber-Institut der MPG, Phys. Chemie, Faradayweg 4-6, 14195 Berlin, Germany, The Blackett Laboratory, Imperial College London, London SW7 2AZ, United Kingdom, U.S. Naval Research Laboratory, Washington, DC, United States, and Department of Electrical and Computer Engineering, National University of Singapore, Singapore

E-mail: razdolski@fhi-berlin.mpg.de; paarmann@fhi-berlin.mpg.de

Abstract

We report on strong enhancement of mid-infrared second harmonic generation (SHG) from SiC nanopillars due to the resonant excitation of localized surface phonon-polaritons within the Reststrahlen band. The magnitude of the SHG peak at the monopole mode experiences a strong

---

[*]To whom correspondence should be addressed
[†]Fritz-Haber-Institut der MPG, Phys. Chemie, Faradayweg 4-6, 14195 Berlin, Germany
[‡]The Blackett Laboratory, Imperial College London, London SW7 2AZ, United Kingdom
[¶]U.S. Naval Research Laboratory, Washington, DC, United States
[§]Department of Electrical and Computer Engineering, National University of Singapore, Singapore
[‖]Department of Electrical and Computer Engineering, National University of Singapore, Singapore

dependence on the resonant frequency beyond that described by the field localization degree and the dispersion of linear and nonlinear-optical SiC properties. Comparing the results for the identical nanostructures made of 4H and 6H SiC polytypes, we demonstrate the interplay of localized surface phonon polaritons with zone-folded weak phonon modes of the anisotropic crystal. Tuning the monopole mode in and out of the region where the zone-folded phonon is excited in 6H-SiC, we observe a prominent increase of the already monopole-enhanced SHG output when the two modes are coupled. Envisioning this interplay as one of the showcase features of mid-infrared nonlinear nanophononics, we discuss its prospects for the effective engineering of nonlinear-optical materials with desired properties in the infrared spectral range.

Light localization in sub-wavelength volumes is a core of modern nanophotonics. Conventional methods of achieving strong confinement of the electromagnetic fields extensively utilize unique properties of surface plasmons. A remarkable variety of objects and materials supporting these excitations ensures the key role of plasmonics in a broad range of applications.[1–5] Apart from unparalleled sensitivity of plasmonic structures to the optical properties of the environment, strong light localization facilitates nonlinear-optical effects.[6–8] Owing to the spectral tunability of the localized plasmon resonances and their sizeable nonlinearity, metallic nanostructures of different shapes and sizes have earned their place in nonlinear photonics.

Despite obvious advantages of plasmon-based nanophotonics, metallic nanoobjects exhibit significant optical losses, which lower the quality factor of the localized surface plasmon modes. Fast plasmon damping (typically on the order of 10 fs) due to ohmic losses[9,10] thus inhibits nonlinear-optical conversion. An alternative, promising metal-free approach has been suggested, utilizing polar dielectrics such as SiC[11–15] or BN[16–20] for high-quality light confinement in the mid-infrared (IR). In these materials, the subdiffractional confinement of electromagnetic radiation relies upon surface phonon polaritons (SPhP) in the Reststrahlen band: the electric polarization is created due to coherent oscillations of the ions instead of the electron or hole densities. Due to the significantly longer scattering times associated with optical phonons as compared to surface plasmons, the lifetimes of SPhPs tend to be on the order of picoseconds, much longer than their plasmonic
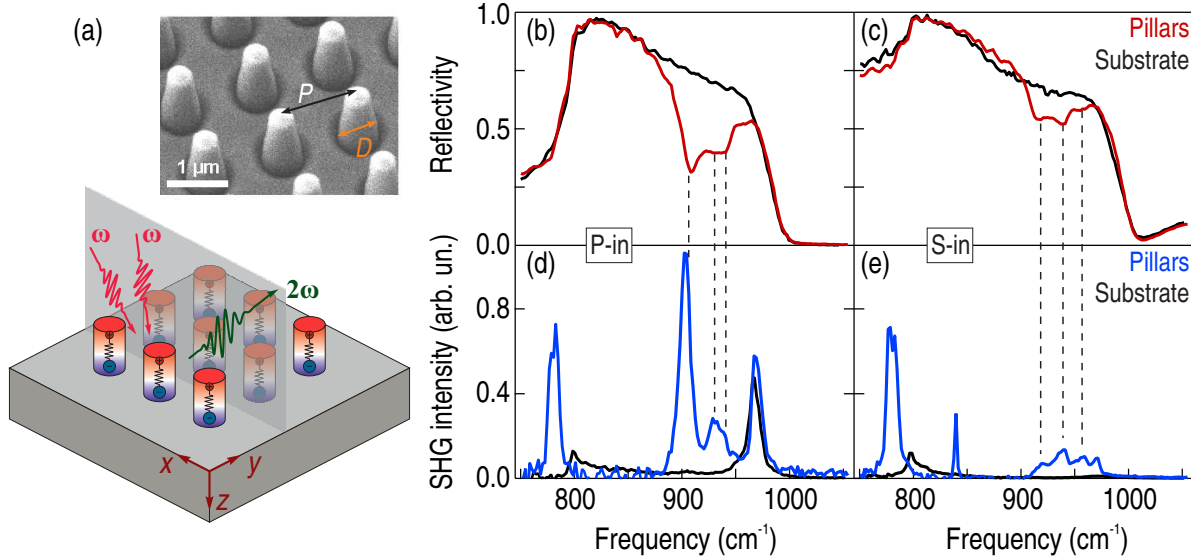
2

Figure 1: (a) Schematic of the experimental approach. The inset shows an electron microscopy image of the nanopillar array. (b-c) Linear reflectivity spectra for *p*- and *s*-polarised incident radiation obtained on the array of 4H-SiC nanopillars (red) and on the 4H-SiC substrate (black). (d-e) SHG output spectra on the 4H-SiC nanopillars (blue) and the 4H-SiC substrate (black). The vertical dashed lines indicate the excited eigenmodes of the pillars.

counterparts.[21] In addition, due to energies associated with optical phonons, SPhPs with typical frequencies within the mid-IR ($> 6\mu m$) to the THz domain hold high promise for spectroscopic and nanophotonic applications.[22–24]

In this Letter, we undertake a first step towards the largely unexplored domain of mid-IR nonlinear nanophononics. We study the nonlinear-optical response of localized SPhPs using nanostructures made of different polytypes of SiC. Using free electron laser (FEL) radiation in the mid-IR spectral range,[25] we probe second harmonic generation from rectangular arrays of subdiffractional, cylindrical SiC nanopillars. The SHG yield in the Reststrahlen band of SiC demonstrates prominent enhancement at the wavelengths associated with the excitation of the SPhP eigenmodes of the pillars. Depending on both the size and the spatial periodicity of the pillars, the SHG-probed eigenmode exhibits a spectral shift accompanied with strong variations of the SHG intensity. Analyzing different SiC polytypes, we demonstrate the interplay of the localized SPhPs with the zone-folded optical phonon modes. We further conclude that strong coupling of the two modes allows for a significant additional modulation of the SPhP-enhanced SHG output.

3

The schematic of our experimental approach is outlined in Fig. 1,a. We employed a non-collinear SHG configuration discussed elsewhere[26] to perform spectroscopic SHG measurements on square arrays of 1 μm-tall 4H-SiC and 6H-SiC pillars with the main axis of the arrays in the *xz* plane of incidence. The fundamental radiation incident at 28 and 62 degrees with respect to the normal to the sample surface was focused onto the sample with a peak fluence on the order of 10 mJ/cm^2. Both 4H and 6H-SiC samples were c-cut so that the *c*-axis of the crystals was parallel to the surface normal. Typical SHG and linear reflectivity spectra collected using the FEL radiation for the two incident polarisations are presented in Fig. 1,b-e. There, the respective spectra of the bare substrate are shown for comparison. For *p*-polarised fundamental radiation (Fig. 1,d), the SHG response features two pronounced peaks located at the zone-center frequencies of transverse and longitudinal optical phonons in SiC,[26] around 797 cm^{-1} and 965 cm^{-1}, respectively. The corresponding SHG spectrum from the nanopillars demonstrate a much stronger SHG signal at around 900 cm^{-1}. Due to the absence of this peak in the SHG spectrum when the fundamental radiation is *s*-polarised , we attribute this SHG feature to the excitation of the monopole SPhP mode in the nanopillars.[15]

In general, the outgoing SHG field $\vec{E}^{2\omega}$ is related to the incident electromagnetic fields E_i^{ω} via the so-called local field factors L_i^{ω}:

$$E_i^{2\omega} \propto \mathscr{P}_i^{2\omega} = \chi_{ijk}^{(2)} : (L_j^{\omega} E_j^{\omega})(L_k^{\omega} E_k^{\omega}), \tag{1}$$

where $\mathscr{P}_i^{2\omega}$ is the nonlinear polarisation and $\chi_{ijk}^{(2)}$ is the nonlinear susceptibility tensor. The excitation of the SPhP monopole mode leads to strong localization of the *z*-projection of the fundamental electric field E_z (normal to the surface plane) and thus a resonant enhancement of L_z^{ω}. The latter results in a pronounced increase of the SHG output when the fundamental radiation is *p*-polarised. However, the SPhP dipole modes observed in the range of 920–960 cm^{-1} rely on the resonant enhancement of the in-plane electric fields described by the local field factors $L_{x,y}^{\omega}$ and thus can be excited with both *p*- and *s*-polarised fundamental radiation. The total SHG response is given by a vector sum of the terms on the right hand side of Eq. (1) originating from various tensor com-

ponents of the nonlinear susceptibility $\chi^{(2)}$. As the strength of $\chi^{(2)}_{zzz}$ is the largest in this spectral range,[27] the SPhP monopole mode, with an enhancement of L^{ω}_z, naturally results in a higher SHG output than the dipole modes.

The results of the systematic studies of the SHG response of various arrays of nanopillars are summarized in Fig. 2 for the 4H-SiC (a,c) and 6H-SiC (b,d) samples. The panels (a-b) illustrate the evolution of the SHG spectra upon varying pillar diameter D. It is seen that upon decreasing D, the SPhP monopole-driven SHG peak exhibits a clear redshift. Remarkably, while the SPhP monopole mode shifts in the range of about 890-910 cm^{-1}, the SHG enhancement factor associated with the excitation of the SPhP monopole mode varies strongly with D. The panels (c-d) offer a zoom-in into the evolution of the SPhP monopole mode-driven SHG for a large variety of nanopillar arrays, indicating that the variations of the SHG enhancement are observed for both 4H and 6H samples. The dependences of the SPhP monopole-driven SHG output on the spectral position of the SPhP monopole mode for the two SiC polytypes are shown in Fig. 3,a with open symbols.
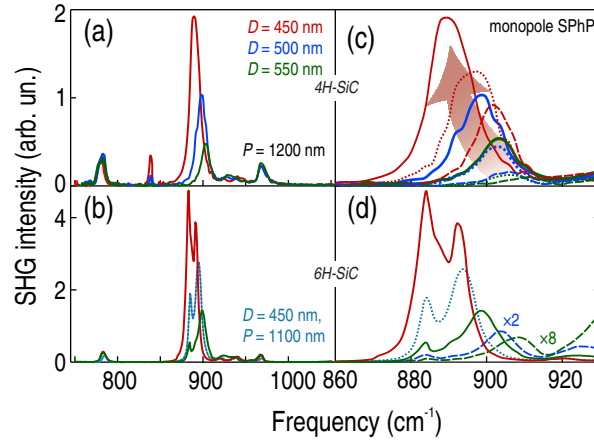

Figure 2: Experimental p-in SHG spectra for three different values of the pillar diameter D for the 4H-SiC (a) and 6H-SiC (b) samples. (c-d) Zoom-in into the SHG spectra in the vicinity of the SPhP monopole resonance. Here, the colours are the same as in (a,b), and solid, dotted, and dashed lines represent $P = 1200$, 1100 and 1000 nm, respectively.

The strong dispersion in the SiC Reststrahlen band suggests that the observed spectral dependence of the SHG enhancement could be captured in numerical simulations. We calculated SHG response using both linear and nonlinear SiC dispersion,[14,26,27] the results of the simulation of the linear optical response,[15] and nonlinear polarization $\mathscr{P}^{2\omega}$ from Eq. (1) spatially integrated over
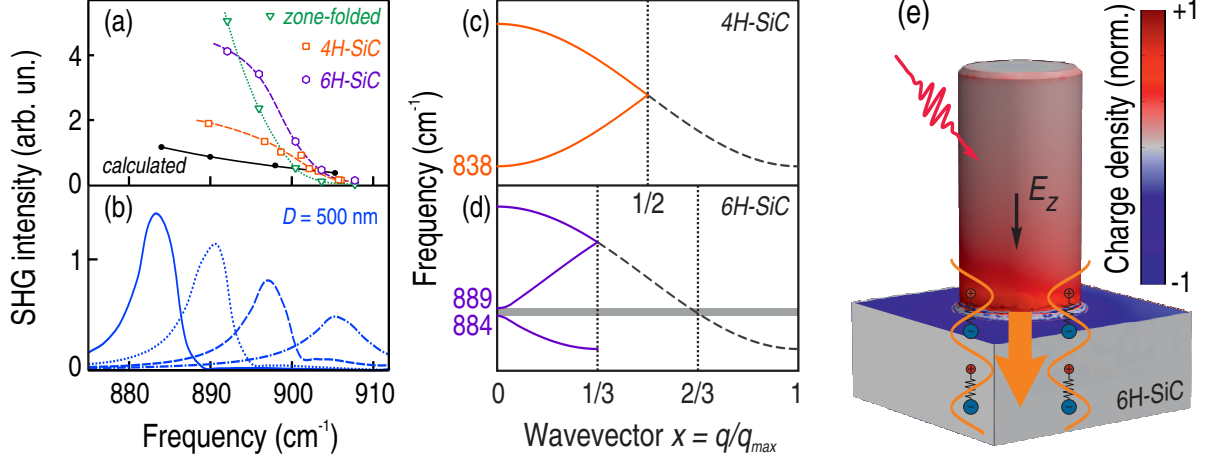
5

Figure 3: (a) Variations of the resonant SHG output with the fundamental frequency of the SPhP monopole mode. The data for both 4H-SiC (red squares) and 6H-SiC (blue circles)demonstrate enhancement of the SPhP monopole resonance-driven SHG when the frequency of the SPhP mode is red-shifted. The full black circles indicate the expected SHG output modulation, as obtained from the numerical simulations (b). The green triangles demonstrate the increase of the SHG output driven by the excitation of the zone-folded mode in 6H-SiC samples. (b) Numerically simulated SHG output spectra in the vicinity of the SPhP monopole mode for the pillar diameter D=500 nm and four different array periodicities $P = 900$, 1000, 1100 and 1200 nm. (c-d) Sketch of the dispersion of the longitudinal optical phonon modes in the full Brillouin zone and the emergence of the zone-folded modes in 4H- and 6H-SiC polytypes. (e) Illustration of the coupling mechanism of the zone-folded and the monopole SPhP modes via the enhanced normal to surface projection of the electric field E_z. The false colour map in the background represents the calculated distribution of the electric charge when the SPhP monopole mode is excited.

the SiC volume, with the following non-zero components of the nonlinear susceptibility: $\chi^{(2)}_{zzz}$, $\chi^{(2)}_{zxx}$ and $\chi^{(2)}_{xxz} = \chi^{(2)}_{xzx}$. The resultant SHG spectra simulated with COMSOL multiphysics software (www.comsol.com) are shown in Fig. 3,b with full symbols. It is seen that the steep experimental dependence cannot be quantitatively described within the simple model used in the calculations, which yields only a moderate increase of the SHG output when the SPhP monopole mode frequency is decreased.

We note the work of Carpetti et al.[28] where the authors thoroughly examined plasmon-induced SHG enhancement from arrays of Au nanoparticles as a function of the inter-particle distance b. In the regime of $b < \lambda$ (as it is in our case), the dependence of the SHG output on b was explained in terms of the changing filling factor (and thus the associated number of active nanoemitters). For very small inter-particle gaps ($b/\lambda \sim 10^{-2}$), a modulation of the SHG output has been attributed to

6

the modification of the electromagnetic field localization in the gaps.[29] Further, a large mismatch between the spatial period of the nanopillars $P \sim 1 \mu m$ and the resonant light wavelength $\lambda \sim 10 \mu m$ rules out the excitation of propagating surface polaritons[30] which are known to enhance the SHG output.[31–35] Since all these effects are included in our simulations, we conclude that the origin of the observed SHG enhancement is unrelated to the periodicity of the array.

An alternative scenario for the observed trend could invoke modifications of the non-local SHG contribution enhanced by a regular array structure. The importance of the non-local SHG was already demonstrated in a number of subwavelength-separated plasmonic nanoobjects.[29,36–42] The amplitude and phase of this non-local SHG source depends on the electric field distribution, i.e. on both the pillar size D and the periodicity P. As such, the interference conditions between the SHG sources vary for different samples, thus resulting in a strong modification of the SHG output.

Further, the apparent difference in the shape of the resonant SHG output for the 4H and 6H samples (see Fig. 2) is related to the anisotropic nature of SiC. The hexagonal SiC polytypes are known to exhibit zone-folded weak modes in the Reststrahlen region[43] originating from particular stacking of the atomic layers along the c-axis of the crystal.[44,45] These weakly IR-active zone-folded modes can be visualised in the reflectivity measurements at oblique incidence.[46] Although zone-folded modes exist in both 4H and 6H polytypes, different stacking of the SiC atomic layers is responsible for them having different frequencies, as illustrated in Fig. 3,c-d. The additional periodicity in the crystal results in folding of the large Brillouin zone thus modifying the phonon dispersion and making the excitation of phonons with non-zero wavevectors ($q \neq 0$) possible. It is seen in Fig. 3,d that the zone-folded mode in the 6H-SiC polytype with the reduced wavevector $q = 2/3 \, \pi/a$ can be excited in the range of $880 - 890 \; \mathrm{cm}^{-1}$ which is close to the typical monopole SPhP resonant frequency of the SiC nanopillars discussed above. In particular, the interaction of the SPhP and zone-folded mode which shifted the apparent spectral positions of the monopole SPhP eigenmode in the linear response,[14] is seen responsible for the complex structure of the resonant SHG output in our experiments (Fig. 2,d). The weak IR activity of the zone-folded modes

is related to the large negative dielectric permittivity of SiC in the Reststrahlen band. As such, the out-of-plane component of the electromagnetic field E_z remains small which inhibits the coupling of incident light to the zone-folded phonon mode. However, the excitation of the SPhP monopole mode in the nanopillars drives a strong increase of E_z, which facilitates the SPhP monopole interaction with the zone-folded phonon (Fig. 3,c).

Figure 3,a illustrates the effect of the zone-folded mode on the observed SHG output. The open red squares (4H) and blue circles (6H) depict the SHG intensity obtained at the SPhP monopole (resonant) frequencies, and the dashed lines illustrate a clear correlation between the maximum SHG output and the spectral position of the SPhP monopole peak. Similar trends are observed for the 4H and 6H-SiC samples as long as the SPhP monopole and the zone-folded mode are well-separated. When these two resonances start to overlap, an additional enhancement of the SHG output produced at the SPhP monopole resonance in 6H-SiC samples is observed. Moreover, the dependence of the SHG signal at the frequency of the zone-folded mode 884 cm^{-1} (green triangles) exhibits a much faster increase when the two resonances are brought together (dotted line), indicating an efficient interplay between the SPhP monopole and the zone-folded mode.

We note that the interaction of the localized SPhP eigenmodes and the intrinsic excitations of the medium is a unique fingerprint of mid-IR nanophononics. Indeed, surface plasmon excitations in metals rely on the free electron gas, which is essentially isotropic. As such, the SHG output of plasmonic nanostructures is (i) largely determined by the metal of choice, usually Au, (ii) exhibits only weak spectral dependence[28,47] and (iii) is limited by robust phase relations in the likely case of multiple SHG sources.[41,48–51] On the contrary, the flexibility of the SPhPs is provided by the coupling of the surface phonon polariton excitations to the intrinsic bulk phonon modes. The latter can be engineered by designing artificial metamaterials based on hybrid multilayer structures,[52,53] thus allowing for an effective control of their optical properties.

To summarize, we have observed SHG output enhancement associated with the excitation of the SPhP eigenmodes in an array of nanopillars grown from SiC of different polytypes. The strongest SHG output is associated with the excitation of the monopole SPhP mode characterized

by strong localization of the normal to surface projection of the electric field E_z. The spectral positions of the SHG peaks shift according to the geometric parameters of the nanophononic structures. We found a strong dependence of the magnitude of the SHG enhancement on the resonant frequency. This experimentally observed dependence cannot be quantitatively described by simply taking into account the sub-diffractional field localization and the dispersion of the linear and nonlinear optical properties of SiC. Further, we discuss the interplay of the SPhPs and the intrinsic crystalline anisotropy for an efficient nonlinear-optical conversion. This mechanism is supported by the SHG spectral measurements on the 6H-SiC nanopillars where excitation of the SPhP monopole mode interacting with the weak zone-folded phonon resulted in an additional enhancement of the SHG output. The presence of intrinsic resonances strongly alters the phase relations in their vicinity, providing a natural way for optimizing the SHG response in a relatively narrow spectral range. Our findings demonstrate high potential of mid-IR nonlinear nanophononics as a novel and promising platform for nonlinear optics and illustrate the rich opportunities it provides for efficient control over nonlinear-optical response.

Acknowledgement

Supplementary Information:

Numerical simulations

The simulations we discuss here allowed us to obtain spectra of the SHG response. We employed COMSOL multiphysics software (www.comsol.com) in order to perform simulations of the linear

optical response as described in Ref.[15] A unit cell containing a single SiC pillar attached to the SiC substrate was constructed, with Floquet boundary conditions along the x-axis and periodic boundary conditions along the y-axis, perpendicular to the plane of incidence. A p-polarized plane wave at frequency ω was launched towards the SiC structure at an incident angle of $25°$. Originating from the p-polarised light source, the electric field $\vec{E}$ inside the SiC pillar and substrate was recorded. Then, this electric field was translated into the nonlinear polarization $\mathscr{P}^{2\omega}$, according to Eq. (1) in the main Manuscript. There, the following non-zero components of the nonlinear susceptibility were accounted for: $\chi_{zzz}^{(2)}$, $\chi_{zxx}^{(2)}$ and $\chi_{xxz}^{(2)} = \chi_{xzx}^{(2)}$.

As a next step, $\mathscr{P}^{2\omega}$ in the pillar and the substrate was regarded as the source of scattered electric field $E^{2\omega}$ inside the unit cell. The SHG output was then obtained by integrating the power flow through a xy-plane set above the substrate. Sweeping the fundamental frequency and taking the dispersion of both linear and nonlinear SiC susceptibilities from Refs.,[14,26,27] we calculated several SHG spectra for samples with various periodicity of the pillars. We note that in these calculations, the input power density at fundamental frequency was kept constant, and the SHG output power was normalized to the area of the xy-plane $S \propto P^2$. The results of the simulations presented in Fig. 3 in the main Manuscript demonstrate a single pronounced peak corresponding to the excitation of the SPhP monopole mode.

References

(1) Barnes, W. L.; Dereux, A.; Ebbesen, T. W. Surface plasmon subwavelength optics. *Nature (London)* **2003**, *424*, 824–830

(2) Maier, S. A. *Plasmonics: Fundamentals and Applications*; Springer: New York, 2007

(3) Schuller, J. A.; Barnard, E. S.; Cai, W.; Jun, Y. C.; White, J. S.; Brongersma, M. L. Plasmonics for extreme light concentration and manipulation. *Nat. Mater.* **2010**, *9*, 193–204

(4) Boriskina, S. V.; Ghasemi, H.; Chen, G. Plasmonic materials for energy: From physics to applications. *Mater. Today* **2013**, *16*, 375–386

(5) Brongersma, M. L.; Halas, N. J.; Nordlander, P. Plasmon-induced hot carrier science and technology. *Nat. Nano.* **2015**, *10*, 25–34

(6) Kauranen, M.; Zayats, A. V. Nonlinear Plasmonics. *Nat. Photon.* **2012**, *6*, 737–748

(7) Hentschel, M.; Utikal, T.; Metzger, B.; Giessen, H.; Lippitz, M. In *Progress in Nonlinear Nano-Optics*; Sabake, S., Lienau, C., Grunwald, R., Eds.; Springer International Publishing: Switzerland, 2015; Chapter 9, pp 153–181

(8) Butet, J.; Brevet, P.-F.; Martin, O. J. F. Optical Second Harmonic Generation in Plasmonic Nanostructures: From Fundamental Principles to Advanced Applications. *ACS Nano* **2015**, *9*, 10545–10562

(9) Vahala, K. J. Optical microcavities. *Nature (London)* **2003**, *424*, 839–846

(10) Barnes, W. L. Surface plasmon-polariton length scales: a route to sub-wavelength optics. *J. Opt. A: Pure Appl. Opt.* **2006**, *8*, S87–S93

(11) Greffet, J.-J.; Carminati, R.; Joulain, K.; Mulet, J.-P.; Mainguy, S.; Chen, Y. Coherent emission of light by thermal sources. *Nature (London)* **2002**, *416*, 61–64

(12) Hillenbrand, R.; Taubner, T.; Keilmann, F. Phonon-enhanced light-matter interaction at the nanometre scale. *Nature (London)* **2002**, *418*, 159–162

(13) Neuner III, B.; Korobkin, D.; Fietz, C.; Carole, D.; Ferro, G.; Shvets, G. Critically coupled surface phonon-polariton excitation in silicon carbide. *Opt. Expr.* **2007**, *34*, 2667–2669

(14) Caldwell, J. D.; Glembocki, O. J.; Francescato, Y.; Sharac, N.; Giannini, V.; Bezares, F. J.; Long, J. P.; Owrutsky, J. C.; Vurgaftman, I.; Tischler, J. G.; Wheeler, V. D.; Bassim, N. D.; Shirey, L. M.; Kasica, R.; Maier, S. A. Low-Loss, Extreme Subdiffraction Photon Confinement via Silicon Carbide Localized Surface Phonon Polariton Resonators. *Nano Lett.* **2013**, *13*, 3690–3697

(15) Chen, Y.; Francescato, Y.; Caldwell, J. D.; Giannini, V.; Maß, T. W. W.; Glembocki, O. J.; Bezares, F. J.; Taubner, T.; Kasica, R.; Hong, M.; Maier, S. A. Spectral tuning of localized surface phonon polariton resonators for low-loss mid-IR applications. *ACS Photonics* **2014**, *1*, 718–724

(16) Caldwell, J. D.; Kretinin, A. V.; Chen, Y.; Giannini, V.; Fogler, M. M.; Francescato, Y.; Ellis, C. T.; Tischler, J. G.; Woods, C. R.; Giles, A. J.; Hong, M.; Watanabe, K.; Taniguchi, T.; Maier, S. A.; Novoselov, K. S. Sub-diffractional volume-confined polaritons in the natural hyperbolic material hexagonal boron nitride. *Nat. Commun.* **2014**, *5*, 5221

(17) Dai, S. et al. Tunable phonon polaritons in atomically thin van der Waals crystals of boron nitride. *Science* **2014**, *343*, 1125–1129

(18) Caldwell, J. D.; Vurgaftman, I.; Tischler, J. G. Probing hyperbolic polaritons. *Nat. Photon.* **2015**, *9*, 638–640

(19) Li, P.; Lewin, M.; Kretinin, A. V.; Caldwell, J. D.; Novoselov, K. S.; Taniguchi, T.; Watanabe, K.; Gaussmann, F.; Taubner, T. Hyperbolic phonon-polaritons in boron nitride for near-field optical imaging and focusing. *Nat. Commun.* **2015**, *6*, 7507

(20) Dai, S.; Ma, Q.; Andersen, T.; McLeod, A. S.; Fei, Z.; Liu, M. K.; Wagner, M.; Watanabe, K.; Taniguchi, T.; Thiemens, M.; Keilmann, F.; Jarillo-Herrero, P.; Fogler, M. M.; Basov, D. N. Subdiffractional focusing and guiding of polaritonic rays in a natural hyperbolic material. *Nat. Commun.* **2015**, *6*, 6963

(21) Caldwell, J. D.; Lindsay, L.; Giannini, V.; Vurgaftman, I.; Reinecke, T. L.; Maier, S. A.; Glembocki, O. J. Low-loss, infrared and terahertz nanophotonics using surface phonon polaritons. *Nanophotonics* **2014**, *4*, 44–68

(22) Ferguson, B.; Zhang, X.-C. Materials for terahertz science and technology. *Nat. Photon.* **2002**, *1*, 26–33

(23) Ulbricht, R.; Hendry, E.; Shan, J.; Heinz, T. F.; Bonn, M. Carrier dynamics in semiconductors studied with time-resolved terahertz spectroscopy. *Rev. Mod. Phys.* **2011**, *83*, 543–586

(24) Kampfrath, T.; Tanaka, K.; Nelson, K. A. Resonant and nonresonant control over matter and light by intense terahertz transients. *Nat. Photon.* **2013**, *7*, 680–690

(25) Schöllkopf, W.; Gewinner, S.; Junkes, H.; Paarmann, A.; von Helden, G.; Bluem, H.; Todd, A. M. M. The new IR and THz FEL facility at the Fritz Haber Institute in Berlin. *Proc. SPIE* **2015**, *9512*, 95121L

(26) Paarmann, A.; Razdolski, I.; Melnikov, A.; Gewinner, S.; Schöllkopf, W.; Wolf, M. Second harmonic generation spectroscopy in the Reststrahl band of SiC using an infrared free-electron laser. *Appl. Phys. Lett.* **2015**, *107*, 081101

(27) Paarmann, A.; Razdolski, I.; Gewinner, S.; Schoellkopf, W.; Wolf, M. Effects of Crystal Anisotropy on Optical Phonon Resonances in the Mid-Infrared Second Harmonic Response of SiC. **2016**, arXiv:1607.05207 [cond–mat.mtrl–sci]

(28) Carpetti, A.; Walsh, G. F.; Minissale, S.; Trevino, J.; Forestiere, C.; Miano, G.; Negro, L. D. Multipolar second harmonic generation from planar arrays of Au nanoparticles. *Opt. Expr.* **2012**, *20*, 15797–15806

(29) Canfield, B. K.; Husu, H.; Laukkanen, J.; Bai, B.; Kuittinen, M.; Turunen, J.; Kauranen, M. Local Field Asymmetry Drives Second-Harmonic Generation in Noncentrosymmetric Nanodimers. *Nano Lett.* **2007**, *7*, 1251–1255

(30) Raether, H. *Surface Plasmons on Smooth and Rough Surfaces and on Gratings*; Springer-Verlag: Berlin, 1988

(31) Agarwal, G. S.; Jha, S. S. Surface-enhanced second-harmonic generation at a metallic grating. *Phys. Rev. B* **1982**, *26*, 482

(32) Coutaz, J. Experimental study of second-harmonic generation from silver gratings of various groove depths. *J. Opt. Soc. Am. B* **1987**, *4*, 105–106

(33) Quail, J. C.; Simon, H. J. Second-harmonic generation from a silver grating with surface plasmons. *J. Opt. Soc. Am. B* **1988**, *5*, 325–329

(34) Razdolski, I.; Parchenko, S.; Stupakiewicz, A.; Semin, S.; Stognij, A.; Maziewski, A.; Kirilyuk, A.; Rasing, T. Second-Harmonic Generation from a Magnetic Buried Interface Enhanced by an Interplay of Surface Plasma Resonances. *ACS Phot.* **2015**, *2*, 20–26

(35) Gubbin, C. R.; Martini, F.; Politi, A.; Maier, S. A.; De Liberato, S. Strong and Coherent Coupling between Localized and Propagating Phonon Polaritons. *Phys. Rev. Lett.* **2016**, *116*, 246402

(36) Shan, J.; Dadap, J.; Stiopkin, I.; Reider, G.; Heinz, T. Experimental study of optical second-harmonic scattering from spherical nanoparticles. *Phys. Rev. B* **2006**, *73*, 023819

(37) Kujala, S.; Canfield, B. K.; Kauranen, M.; Svirko, Y.; Turunen, J. Phonon-enhanced light-matter interaction at the nanometre scale. *Phys. Rev. Lett.* **2007**, *98*, 167403

(38) Bachelier, G.; Butet, J.; Russier-Antoine, I.; Jonin, C.; Benichou, E.; Brevet, P.-F. Origin of optical second-harmonic generation in spherical gold nanoparticles: Local surface and nonlocal bulk contributions. *Phys. Rev. B* **2010**, *82*, 235403

(39) Butet, J.; Bachelier, G.; Russier-Antoine, I.; Jonin, C.; Benichou, E.; Brevet, P.-F. Interference between Selected Dipoles and Octupoles in the Optical Second-Harmonic Generation from Spherical Gold Nanoparticles. *Phys. Rev. Lett.* **2010**, *105*, 077401

(40) Razdolski, I.; Gheorghe, D. G.; Melander, E.; Hjörvarsson, B.; Patoka, P.; Kimel, A. V.; Kirilyuk, A.; Papaioannou, E. T.; Rasing, T. Nonlocal nonlinear magneto-optical response of a magnetoplasmonic crystal. *Phys. Rev. B* **2013**, *88*, 075436

(41) Kruk, S.; Weismann, M.; Bykov, A. Y.; Mamonov, E. A.; Kolmychek, I. A.; Murzina, T.; Panoiu, N. C.; Neshev, D. N.; Kivshar, Y. S. Enhanced Magnetic Second-Harmonic Generation from Resonant Metasurfaces. *ACS Photonics* **2015**, *2*, 1007–1012

(42) Hille, A.; Moeferdt, M.; Wolff, C.; Matyssek, C.; Rodriguez-Oliveros, R.; Prohm, C.; Niegemann, J.; Grafstrom, S.; Eng, L. M.; ; Busch, K. Second Harmonic Generation from Metal Nano-Particle Resonators: Numerical Analysis On the Basis of the Hydrodynamic Drude Model. *J. Phys. Chem. C* **2016**, *120*, 1163–1169

(43) Bluet, J.; Chourou, K.; Anikin, M.; Madar, R. Weak phonon modes observation using infrared reflectivity for 4H, 6H and 15R polytypes. *Mater. Sci. Eng.* **1999**, *B61–62*, 212–216

(44) Patrick, L. Infrared Absorption in SiC Polytypes. *Phys. Rev.* **1967**, *167*, 809–813

(45) Feldman, D. W.; Parker, Jr., J. H.; Choyke, W. J.; Patrick, L. Phonon Dispersion Curves by Raman Scattering in SiC, Polytypes 3C, 4H, 6H, 15R, and 21R. *Phys. Rev.* **1968**, *173*, 787–793

(46) Engelbrecht, F.; Helbig, R. Effect of crystal anisotropy on the infrared reflectivity of 6H–SiC. *Phys. Rev. B* **1993**, *48*, 15698–15707

(47) Metzger, B.; Gui, L.; Fuchs, J.; Floess, D.; Hentschel, M.; Giessen, H. Strong Enhancement of Second Harmonic Emission by Plasmonic Resonances at the Second Harmonic Wavelength. *Nano Lett.* **2015**, *15*, 3917–3922

(48) Husu, H.; Canfield, B. K.; Laukkanen, J.; Bai, B.; Kuittinen, M.; Turunen, J.; Kauranen, M. Local-field effects in the nonlinear optical response of metamaterials. *Metamaterials* **2008**, *2*, 155–168

(49) Palomba, S.; Novotny, L. Nonlinear excitation of surface plasmon polaritons by four-wave mixing. *Phys. Rev. Lett.* **2008**, *101*, 056802

(50) Carpetti, A.; Forestiere, C.; Negro, L. D.; Miano, G. Full-Wave Analytical Solution of Second-Harmonic Generation in Metal Nanospheres. *Plasmonics* **2014**, *9*, 151–166

(51) Razdolski, I.; Makarov, D.; Schmidt, O. G.; Kirilyuk, A.; Rasing, T.; Temnov, V. V. Nonlinear Surface Magnetoplasmonics in Kretschmann Multilayers. *ACS Photonics* **2016**, *3*, 179–183

(52) Dai, S. et al. Graphene on hexagonal boron nitride as a tunable hyperbolic metamaterial. *Nat. Nano.* **2015**, *10*, 682–687

(53) Caldwell, J. D.; Vurgaftman, I.; Tischler, J. G.; Glembocki, O. J.; Owrutsky, J. C.; Reinecke, T. L. Atomic-scale photonic hybrids for mid-infrared and terahertz nanophotonics. *Nat. Nano.* **2015**, *11*, 9–15